




Cite this: *Soft Matter*, 2024, 20, 1486

# Understanding the application of covalent adaptable networks in self-repair materials based on molecular simulation†

Xiang Cui,‡ Lu Zhang,‡ Yuliang Yang and Ping Tang \*

Covalent adaptable networks (CANs) are widely used in the field of self-repair materials. They are a group of covalently cross-linked associative polymers that undergo reversible chemical reactions, and can be further divided into dissociative CANs (Diss-CANs) and associative CANs (Asso-CANs). Self-repair refers to the ability of a material to repair itself without external intervention, and can be classified into self-adhesion and self-healing according to the utilization of open stickers. Unlike conventional materials, the viscoelastic properties of CANs are influenced by both the molecular structure and reaction kinetics, ultimately affecting their repair performance. To gain deeper insight into the repair mechanism of CANs, we conducted simulations by using the hybrid MC/MD algorithm, as previously proposed in our research. Interestingly, we observed a significant correlation between reaction kinetics and repair behavior. Asso-CANs exhibited strong mechanical strength and high creep resistance, rendering them suitable as self-adhesion materials. On the other hand, Diss-CANs formed open stickers that facilitated local relaxation, aligning perfectly with self-healing processes. Moreover, the introduction of crosslinkers in the form of small molecules enhanced the repair efficiency. Theoretically, it was found that the repair timescale of Asso-CANs is slower than that of Diss-CANs with identical molecular structures. Our study not only clarifies the similarities and differences between Diss-CANs and Asso-CANs in terms of their self-repairing capabilities, but more importantly, it provides valuable insights guiding the effective utilization of CANs in the development of self-repair materials.

Received 11th October 2023,  
Accepted 11th January 2024

DOI: 10.1039/d3sm01364b

[rsc.li/soft-matter-journal](http://rsc.li/soft-matter-journal)

## 1. Introduction

Self-repair refers to the capability of a material to autonomously repair its own damage or defects. This process is commonly observed in biological systems, such as the natural healing of human skin injuries, the regeneration of damaged organs in animals, and the grafting process in plants. Inspired by nature, self-repair materials exhibit great prospects in fields like biomedical treatment,<sup>1–3</sup> materials engineering,<sup>4–6</sup> and environmental protection.<sup>7–9</sup> The self-repairing process can be achieved either by intrinsic structural changes within the material itself, which mostly rely on inner reversible chemical reactions,<sup>10–14</sup> or by the use of external stimuli or triggers, such as healing agents.<sup>15–17</sup> However, the development of self-repair materials faces challenges in complex chemical synthesis and the design of well-defined self-repairing processes. The key to achieving ideal self-repair materials

lies in the meticulous design of suitable, controllable reversible chemical reactions within the self-repair system. One of the main challenges is the trade-off between mechanical strength and self-repairing capability, as materials typically possess one or the other. Therefore, achieving ideal self-repair materials requires careful design of suitable and controllable reversible chemical reactions within the self-repair system.

Covalent adaptable networks (CANs) are special kinds of associative polymers (APs), which present unique rheological behavior due to the incorporation of dynamic covalent bonds.<sup>18–22</sup> In contrast to traditional polymers, CANs demonstrate outstanding solvent resistance, mechanical properties, and reprocessability. These materials find wide applications in areas such as stimuli responsiveness,<sup>23–25</sup> shape memory,<sup>26–28</sup> molecular transport,<sup>29–31</sup> etc. According to the reaction mechanism, CANs can be further classified into dissociative CANs (Diss-CANs) and associative CANs (Asso-CANs, also known as vitrimers). Diss-CANs undergo reversible sticker dissociation and association, thus leading to the formation of open stickers and the loss of network integrity. In contrast, Asso-CANs only involve bond swap processes, and as a result, the network integrity will be constant. Interestingly, the macroscopic rheology

State Key Laboratory of Molecular Engineering of Polymers, Department of Macromolecular Science, Fudan University, Shanghai 200433, China.  
E-mail: [pingtang@fudan.edu.cn](mailto:pingtang@fudan.edu.cn)

† Electronic supplementary information (ESI) available. See DOI: <https://doi.org/10.1039/d3sm01364b>

‡ X. Cui and L. Zhang contributed equally to this work.



of Asso-CANs shows Arrhenius-type dependence, which is rarely seen in polymers. Owing to the mechanical strength brought by covalent bonding and the controllable inner reversible chemical reactions, CANs are increasingly applied in self-repair materials.<sup>32–36</sup>

On the one hand, these materials exhibit rapid recovery of injured sites while maintaining mechanical strength through rearrangement of polymeric networks. For example, Guo *et al.*<sup>32</sup> proposed a supramolecular elastomer composed of a polydimethylsiloxane (PDMS) polymer backbone embedded with multiple dynamic bonds, including disulfide metathesis, strong crosslinking H-bonds, and weak crosslinking H-bonds. This synergistic interaction enables the material to achieve rapid self-repair while maintaining its mechanical strength. It is shown that the synergistic effects of dynamic bonds endow the elastomer with high stretchability ( $\sim 14\,000\%$ ) as well as fast autonomous self-healing ability under universal conditions, including at room temperature (10 min for healing), ultralow temperature ( $-40\text{ }^{\circ}\text{C}$ ), underwater (93% healing efficiency), super-cooled high-concentrated saltwater (30% NaCl solution at  $-10\text{ }^{\circ}\text{C}$ , 89% efficiency), and a strong acid/alkali environment (pH = 0 or 14, 88% or 84% efficiency).

On the other hand, reversible chemical reactions can be triggered by the temperature, which endows CANs with mechanical strength at room temperature and simultaneously adjustable self-repairing ability when heating.<sup>37</sup> For instance, Leibler *et al.*<sup>33</sup> made a quantitative comparison between permanently cross-linked epoxidized natural rubbers (ENR) and dicarboxylic acids cross-linked ENR (DA (diamine)-cured ENR). They demonstrated that, by introducing transesterification, the ENR cured with DA showed large stress relaxation at high temperatures, while the use of the zinc acetate catalyst promoted the relaxation dynamics. These rubber materials exhibit excellent mechanical properties without undesired creeping at room and moderate temperatures. However, at high temperatures, they also show adhesion and potential healability. Furthermore, the architecture of topological structures of these materials can also provide particular self-repairing capability. Ciarella and Ellenbroek<sup>34</sup> designed star-like vitrimers applied in self-repair coating and found that a single bond swap process was sufficient to build a bridge and stick the damaged surface, while multiple swaps were required to relax the whole network. Apparently, the CANs exhibit excellent mechanical properties under moderate conditions, whereas they also show superior adhesion or healing abilities when subjected to external stimuli, such as heat, pressure, light, *etc.* or in the presence of catalysts. This indicates the controllable repairing ability of CAN materials.

Improving our understanding of the self-repairing process at the molecular level is crucial for designing self-repair materials with tailored functions. However, at present, the interpretation of the chemical and/or physical mechanisms involved in CANs applied in self-healing materials is still insufficient. Rubinstein *et al.*<sup>38</sup> developed scaling theories for self-repair based on hybrid reversible/permanent networks in associative polymers. They emphasize the significance of the match between the

waiting time and relaxation time. Hinton *et al.*<sup>39</sup> extended Rubinstein's model to entangled systems by using a modified filament stretching rheometer. According to these studies, self-adhesion and self-healing are both possible in typical associative polymers. The major difference lies in the presence of open stickers upon damage. When bonded stickers are forced to dissociate, they form a large number of open stickers at the interface. These open stickers are highly active and tend to reassociate with each other, resulting in significant healing effects. Over time, the open stickers become deactivated, transitioning the healing process into adhesion. However, in the case of CANs, the distinction between Diss-CANs and Asso-CANs leads to different adhesion and healing behaviors compared to typical associative polymers. On the basis of the sticky Rouse model,<sup>40–43</sup> the network relaxation of CANs results from the superposition of strand motion and chemical reaction.

We believe that there is always a contradiction between the bulk relaxation of the entire network and the local relaxation on the damaged surface, as they both involve the same chemical reaction. As a result, the structure and kinetics can play a crucial role in determining the repair ability of these materials, which, unfortunately, is challenging to characterize in experiments and is often less emphasized by researchers. Here, to precisely simulate chemical reactions and molecular dynamics simultaneously, we deeply analyze the self-repair behavior of Diss-CANs and Asso-CANs by using the hybrid MC/MD algorithm.<sup>22,38,44–46</sup> By examining the distinct kinetics of these molecular architectures, we present a systematic description of CANs when used for self-repairing. The results of our study demonstrate that the repair ability of CANs is strongly influenced by their structures and kinetics. Our work not only highlights the similarities and differences between Diss-CANs and Asso-CANs in self-repairing applications, but also more importantly, offers valuable insights for guiding the application of CANs in self-repair materials.

The rest of the manuscript is organized as follows. In Section 2, we present detailed hybrid MC/MD algorithms simulating the Diss-CANs and Asso-CANs, and the simulation of their repair process. In Section 3, we analyze the repair process of Diss-CANs and Asso-CANs, evaluating the repair effect by using the triaxial extension. We further discuss the influence of chemical reactions on the repairing kinetics, where the impacts of activation energy and temperature are emphasized. Finally, the conclusions are summarized in Section 4.

## 2. Simulation model and method

We adopt the coarse-grained Kremer–Grest (KG) bead-spring model for presenting polymer networks.<sup>47</sup> A total of 2000 chains with a length of  $N = 5$  and 300 chains with a length of  $N = 50$ , which is at or below the best estimates of the entanglement length  $50 \leq N_e \leq 85$ ,<sup>44,48</sup> are constructed separately in two cubic periodic box with period  $L_i > 2 \langle R_{ee} \rangle$  to ensure that the topological structure of the chain is not affected by the box size. Here  $\langle R_{ee} \rangle$  is the mean end-to-end distance. The choice of box size is to ensure



that further increasing the box size will not influence the final calculation results. The interaction energy between each unbonded monomer employs the Lennard-Jones (LJ) potential energy  $U_{\text{LJ}}$ :

$$U_{\text{LJ}}(r) = 4\epsilon_{\text{LJ}} \left[ \left( \frac{\sigma_{\text{LJ}}}{r} \right)^{12} - \left( \frac{\sigma_{\text{LJ}}}{r} \right)^6 - \left( \frac{\sigma_{\text{LJ}}}{r_c} \right)^{12} + \left( \frac{\sigma_{\text{LJ}}}{r_c} \right)^6 \right] \quad (1)$$

where  $r$  is the distance between monomers and the cutoff radius is  $r_c = 2^{1/6}\sigma_{\text{LJ}}$ , which means the interactions between beads are repulsive. The number density of the LJ beads is  $\rho = 0.85$ . All quantities are expressed in reduced LJ units, including the LJ bead diameter  $\sigma_{\text{LJ}}$ , intermonomer energy  $\epsilon_{\text{LJ}}$ , and the reduced time  $\tau_{\text{LJ}} = \sqrt{m\sigma_{\text{LJ}}^2/\epsilon_{\text{LJ}}}$ . The covalent bonding between neighbor beads is modeled with the finitely extensible nonlinear elastic (FENE) potential as follows:

$$U_{\text{FENE}}(r) = -\frac{1}{2}kR_0^2 \ln \left[ 1 - \left( \frac{r}{R_0} \right)^2 \right] \quad (2)$$

where the spring constant  $k = 30\epsilon_{\text{LJ}}/\sigma_{\text{LJ}}^2$  and the maximum bond length  $R_0 = 1.5\sigma_{\text{LJ}}$ . All of the simulations are performed using the LAMMPS with canonical (NVT) ensemble,<sup>49,50</sup> maintaining the temperature using the Langevin thermostat. Newton's equations of motion are integrated using the velocity-Verlet algorithm.

To highlight the repair effect of CANs, telechelic short chains with 5-mer and crosslinkers such as with four functional groups are firstly constructed, as shown in Fig. 1. Stickers are distributed at the end of each chain and crosslinker, and can only additionally heteroassociate with one other sticker (namely one-to-one) to avoid phase separation. The premixed chains and crosslinkers are cross-linked for  $10^8$  steps to ensure forming a fully cross-linked network. This is the prepared initial network for both Asso-CANs and Diss-CAN.

The hybrid MC/MD algorithm is employed to simulate the reversible network in both Asso-CANs and Diss-CANs. To model Asso-CANs, similar to Perego *et al.*<sup>45,46</sup> and our previous work,<sup>22</sup> we consider that the rearrangement of the network is accomplished *via* bond exchange reactions, ensuring the integrity of the network. When modeling Diss-CANs, we adopt the same approach as Hoy and Fredrickson.<sup>44</sup> In Diss-CANs, the rearrangement of the network depends on the dissociation and

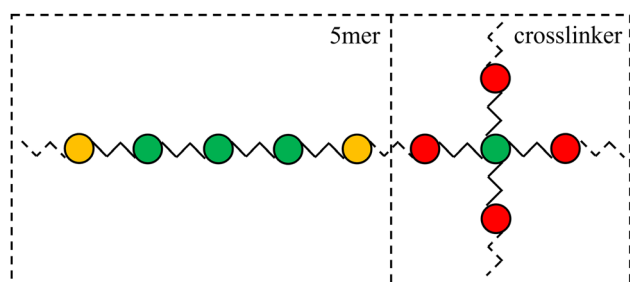


Fig. 1 Schematic description for the molecular structure of the 5-mer and crosslinker with four functional groups. Green circles represent regular beads, yellow circles represent stickers in linear chains, and red circles represent stickers in crosslinkers. Stickers can only additionally bond with one another sticker.

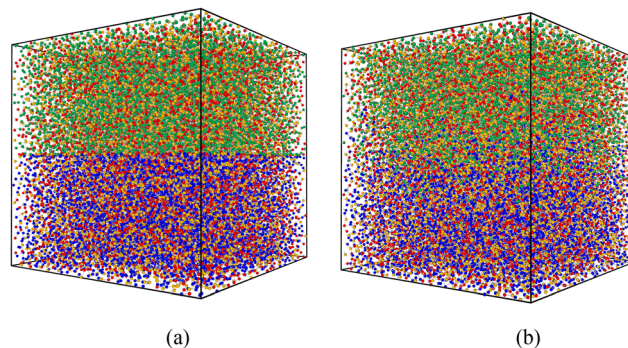


Fig. 2 Snapshots of the simulation box (a) before and (b) after the self-repairing process. The two identical simulation boxes are stacked in the  $z$ -direction with fixed boundary conditions to simulate the damaged interface. The types of beads are the same as Fig. 1. The blue beads represent the regular beads in the box below.

association of stickers, which is simulated through the breaking and creation of sticky bonds. Both methods involve the movement of beads governed by MD equations, while chemical reactions take place in an MC step where the reaction probability is calculated independently.

For the simulation of the repair process, we conducted equilibrium molecular dynamics (EMD) simulations with a timestep of  $\delta t = 0.01\tau_{\text{LJ}}$ . Initially, at  $t = 0$ , two identical simulation boxes are stacked in the  $z$ -direction with fixed boundary conditions to simulate the damaged interface. Subsequently, at  $t = t_1$ , the fixed boundary conditions are converted into periodic boundary conditions to initiate the chemical reaction. The repair process continued until  $t = t_2$ , when the chemical reaction is terminated. The snapshots before and after the repair process are shown in Fig. 2(a) and (b), respectively.

Triaxial stretching along the  $z$ -axis is often used to characterize the repair effect under non-equilibrium molecular dynamics (NEMD) simulation,<sup>51–53</sup> where the tensile stress is expressed by  $P_{zz}$ . Because bond breakage is not allowed in FENE potential, the quartic potential is adopted to obtain the stress-strain curves:

$$U_Q(r) = K(r - R_c)^2(r - R_c)(r - R_c - B) + U_0 \quad (3)$$

where  $K = 2351 \text{ } \epsilon/k_B$ ,  $B = -0.7425\sigma_{\text{LJ}}$ ,  $R_c = 1.5\sigma_{\text{LJ}}$  and  $U_0 = 92.74467\epsilon_{\text{LJ}}$ . The quartic potential has the same balanced bond length as the FENE potential, which has been used in previous simulations<sup>54–57</sup> and confirmed by typical experimental values.<sup>58,59</sup> The extension process is proceeded in periodical boundary conditions with the extension rate  $\dot{\gamma} = 0.01\tau_{\text{LJ}}^{-1}$ .

### 3. Results and discussion

As mentioned above, the self-repairing process involves a competition between the recovery of damaged sites and the overall relaxation of the network. To create a superior self-repair material, it is essential to have both rapid repair ability as well as robust mechanical properties, characterized by fast local site relaxation and slow overall network relaxation.



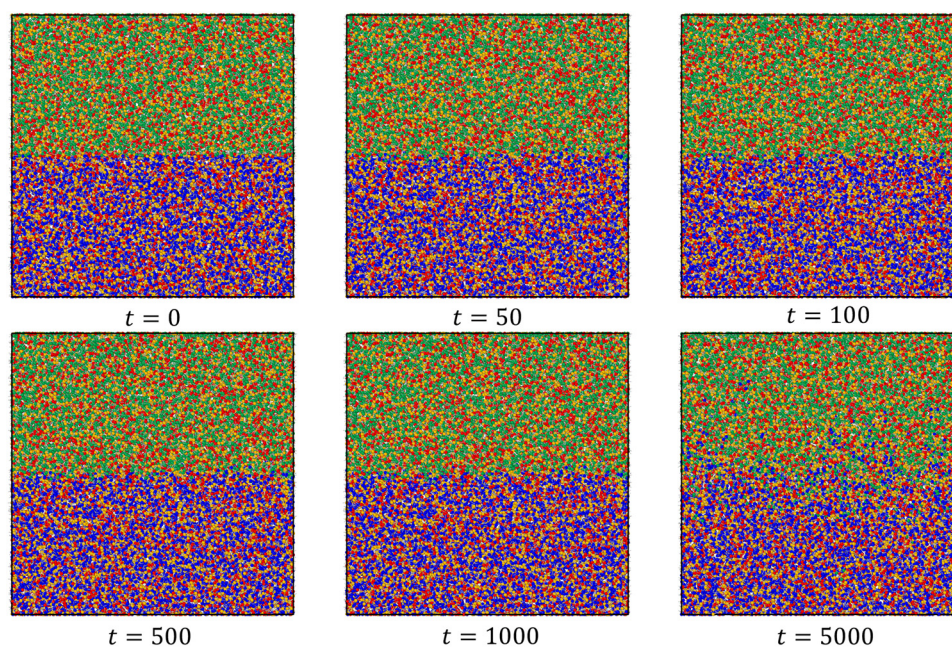


However, conventional CANs face a contradiction in achieving these two kinds of relaxations, as they mainly depend on the same reversible chemical reaction. Indeed, diverse molecular structures and chemical mechanisms are better suited for different types of self-repair behavior based on specific applications and materials. The existence of open stickers further highlights the distinction between self-adhesion and self-healing, making the application of CANs in self-repair materials particularly intriguing.

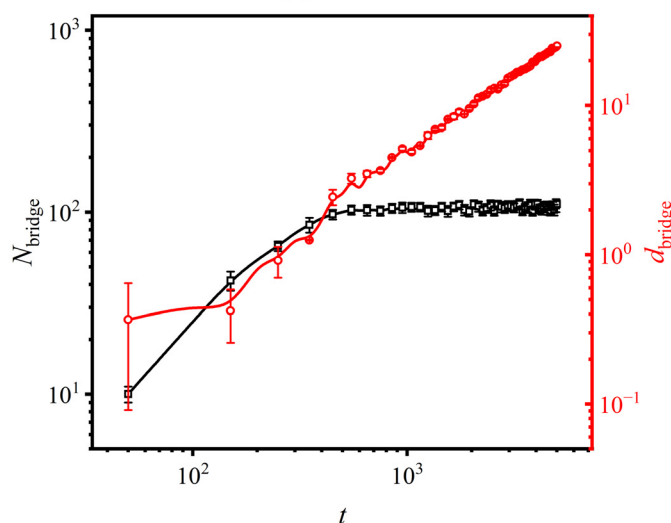
### 3.1. Asso-CAN system suitable for self-adhesion

To achieve self-adhesion such as in coatings, it is desirable to have arbitrary bonding positions and universal bonding

conditions. Homogenous CANs without orientation can easily meet the requirement for sticky positions since chemical reactions can occur everywhere within the network. However, to meet the universal conditions for self-adhesion, the adhesion behavior should be triggered under specific conditions that are relatively easy to achieve and maintain stable behavior under working conditions. To draw an analogy, when using glue, people are willing to wait longer for the glue to cure as long as it provides a strong bond. This means that for self-adhesion, the slower relaxation of the entire network is more important compared to the local relaxation, which is suitable for Asso-CANs because of their conservative crosslinking density.



(a)



(b)

**Fig. 3** (a) Snapshots under different healing times ( $t$ ) in the  $xz$ -plane. (b) The number of bridge chains ( $N_{\text{bridge}}$ ) that connect the two surfaces, and the sticker diffusion depth ( $d_{\text{bridge}}$ ) along the  $z$ -axis, as a function of time ( $t$ ) during adhesion.





We firstly investigate the influence of bond exchange reaction kinetics on self-adhesion. Fig. 3(a) displays snapshots at various healing times. When  $t = 0\tau_{LJ}$ , there is a clear boundary (representing the interface to be bonded) between the two simulation boxes. As adhesion starts, the interface gradually merges and becomes indistinguishable within  $t = 1000\tau_{LJ}$ . The number of bridge chains that connect the two surfaces,  $N_{\text{bridge}}$ , and the depth of sticker diffusion,  $d_{\text{bridge}}$ , are shown in Fig. 3(b). It is found that  $N_{\text{bridge}}$  increases logarithmically with time initially, reaching a maximum at  $t = 500\tau_{LJ}$ , before approaching saturation. Note that the adhesion of Asso-CANs does not need long-distance diffusion, as evidenced by the fact that  $d_{\text{bridge}}$  is only 2% at  $t = 500\tau_{LJ}$ .

The snapshots of the triaxial extension process are shown in Fig. 4(a). When the sample is pulled apart, voids will form in the middle and at the ends of the box. Crack propagation can be clearly observed during triaxial extension. For unstuck samples *i.e.*, with adhesion time  $t = 0\tau_{LJ}$ , the two simulation boxes can be easily separated by an external force. At short times ( $t = 50$  or  $100\tau_{LJ}$ ), bridge chains start forming, but the number of these bridges ( $N_{\text{bridge}}$ ) is too small to effectively hold the two parts together. As the adhesion time increases, the separation between the boxes becomes more difficult. The stress-strain curves in Fig. 4(b) show that the maximum stress for samples with adhesion time  $t \geq 500\tau_{LJ}$  is almost identical to that of the undamaged sample, indicating an excellent adhesion effect.

According to Arrhenius equation:

$$k = A \exp\left(-\frac{E_a^{\text{kin}}}{k_B T}\right) \quad (4)$$

The impact of external stimulus on the self-repairing process can be theoretically observed through the changes in both activation energy and temperature. Therefore, we further explored the adhesion kinetics under various activation energies and temperatures. Fig. 5(a) and (b) show the effect of activation energies on the adhesion processes. With an increase in the adhesion time ( $t$ ),  $N_{\text{bridge}}$  also increases. However, as the activation energies increase, both  $N_{\text{bridge}}$  and  $d_{\text{bridge}}$  experience a significant decrease. This decrease indicates a reduction in the number of bridge chains and the extent of sticker diffusion due to the higher reaction barrier. Consequently, it becomes more difficult for exchange reactions to occur.

The temperature-dependence of the adhesion processes is analyzed in Fig. 5(c) and (d). As the temperature rises,  $N_{\text{bridge}}$  and  $d_{\text{bridge}}$  increase, indicating the acceleration of the exchange reactions. Eqn (4) reveals that the exchange reaction is accelerated at low kinetic activation energies and high temperatures, resulting in an increase in  $N_{\text{bridge}}$  and  $d_{\text{bridge}}$ , which enhance adhesion. When the temperature exceeds a certain threshold ( $T \geq 1.0\epsilon_{LJ}/k_B$ ), the effect of heating on the reactions becomes insignificant. Since crosslinking density remains constant in Asso-CANs, there is a characteristic transition temperature known as the topology freezing temperature ( $T_v$ ), which is above  $T_g$  for commonly used Asso-CANs.  $T_v$  determines whether the

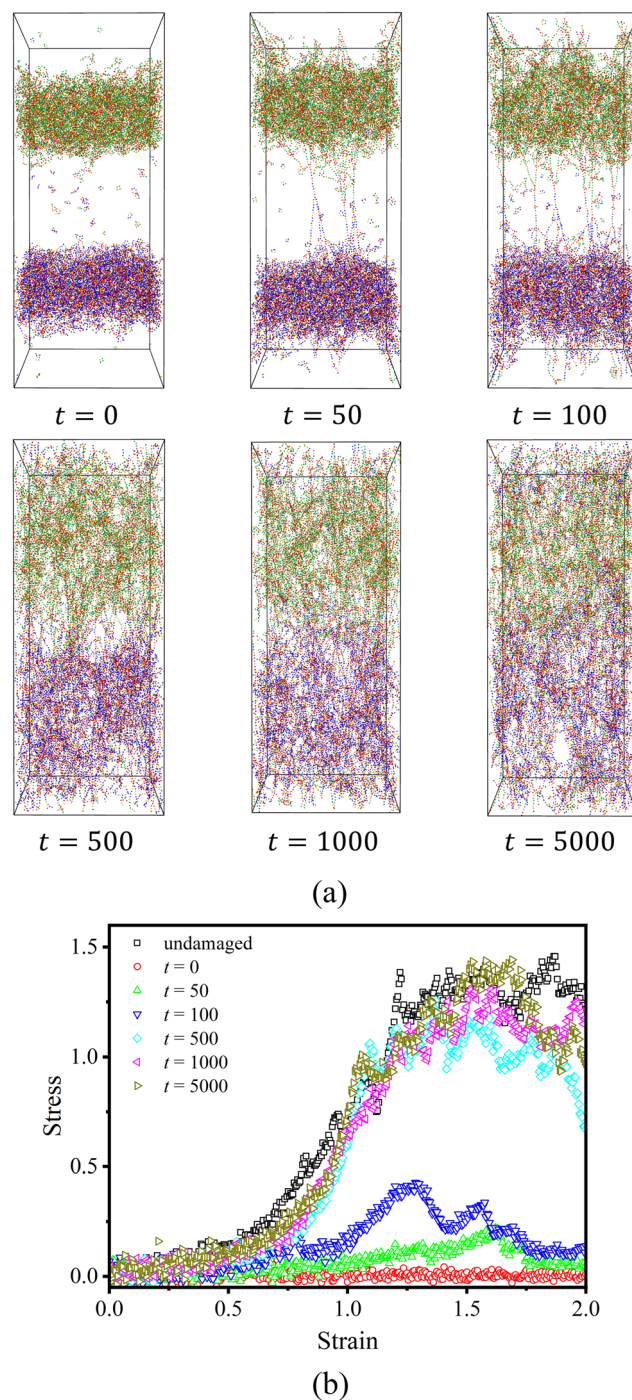


Fig. 4 (a) Extension process snapshots of samples with various adhesion times ( $t$ ). (b) Stress-strain curves of Asso-CANs at various  $t$ . Black symbols (square) represent the original stress-strain curves of the undamaged sample. For clarity, all the statistical points are depicted rather than curves in this paper, and the curves can be obtained by simply connecting a straight line between every set of adjacent points.

bond exchange reaction can proceed. In our simulation, we calculated  $T_v = 0.88\epsilon_{LJ}/k_B$  for Asso-CANs, as shown in Fig. S1 (ESI<sup>†</sup>). Once  $T_v$  is reached, the impact of temperature on the system diminishes. It is noticed that this characteristic actually gives vitrimers an advantage in self-repair applications. As long



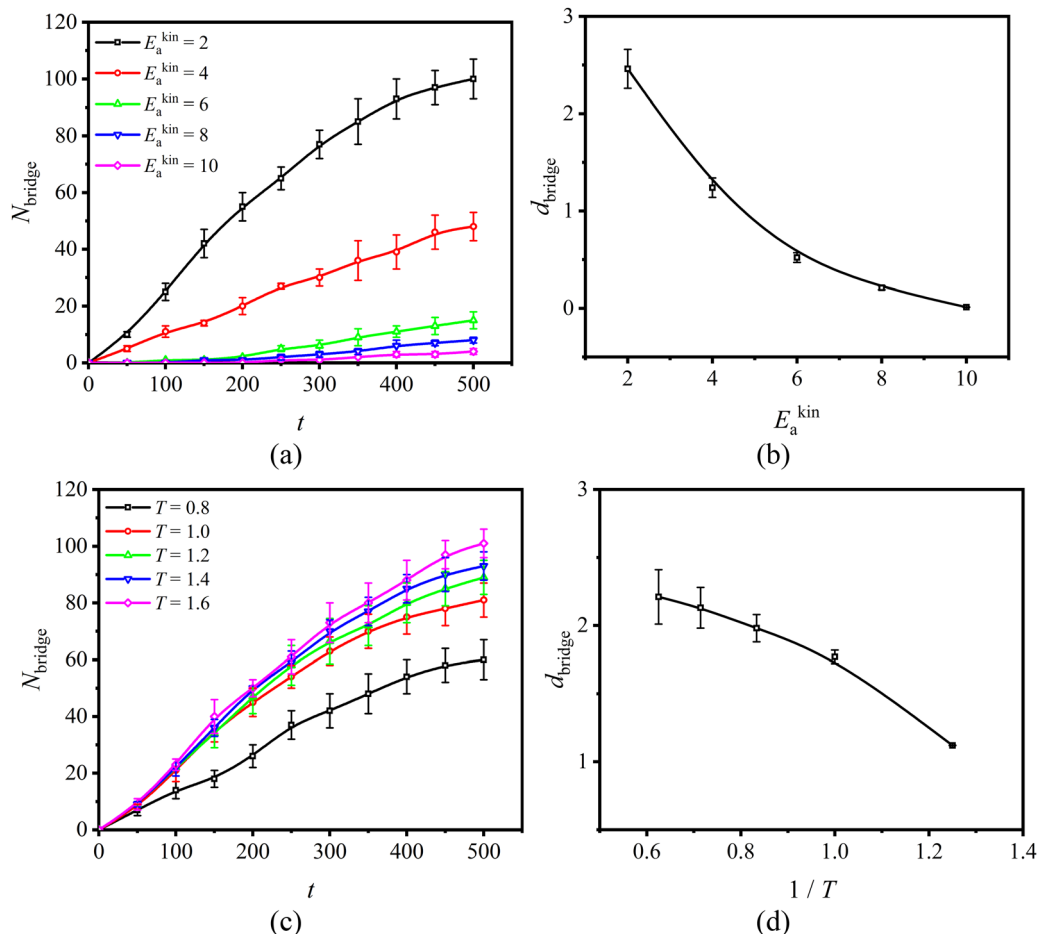


Fig. 5  $N_{\text{bridge}}$  as a function of adhesion time ( $t$ ) at (a) various activation energies ( $E_a^{\text{kin}}$ ) and (c) various temperatures ( $T$ ). Corresponding  $d_{\text{bridge}}$  as a function of (b) activation energy ( $E_a^{\text{kin}}$ ) and (d) temperature ( $T$ ).

as the temperature is above  $T_v$ , the self-repairing process can be triggered.

The triaxial extension is also simulated under different kinetics, and the snapshots at  $t = 500\tau_{\text{LJ}}$  are depicted in Fig. 6(a) and (b). When  $T > 1.0\epsilon_{\text{LJ}}/k_B$ , as time progresses, the two simulation boxes exhibit minimal separation and the stress-strain curves shown in Fig. 6(c) agree with the snapshots. It should be noted that because of the periodic boundary conditions, the repairing behavior in the middle of the box and the boundaries is the same, and as a result, the overall repairing effect should be the synergistic repairing effect of both the parts. For  $T = 1.0\epsilon_{\text{LJ}}/k_B$  in Fig. 6(a), although the bridge chains in the middle of the box seems as many as  $T > 1.0\epsilon_{\text{LJ}}/k_B$ , it showed a worse repairing effect since the bridge chains on boundaries are much fewer than under other conditions. In terms of activation energy, Asso-CANs can be classified into different levels of association strength. According to the snapshots in Fig. 6(b) and the corresponding  $N_{\text{bridge}}$  in Fig. 5(a), at  $t = 500\tau_{\text{LJ}}$ , strong association ( $E_a^{\text{kin}} = 8$  and 10) results in almost no adhesion, while medium association ( $E_a^{\text{kin}} = 4$  and 6) leads to a few bridge chains and poor adhesion performance. However, weak association ( $E_a^{\text{kin}} = 2$ ) shows a vague interface between the

two simulation boxes, and the maximum stress shown in Fig. 6(d) is almost the same as that of the undamaged sample. These results demonstrate that this low activation energy requirement for Asso-CANs is crucial for self-adhesion.

As has been emphasized above, the network relaxation of CANs is due to the superposition of strand motion and chemical reaction. This implies that the calculation of the activation energy for viscous flow, obtained from the terminal relaxation time, involves both the activation energy for strand motion and that for the chemical reaction.<sup>22</sup> It should be noted that the activation energy for viscous flow can be considered as the combined effect of strand motion and chemical reaction based on the mean-field theory. However, when a polymer chain is dynamically crosslinked along the backbone, the mean-field theory becomes inapplicable. Consequently, the viscous activation energy may not be simply considered as the sum of strand motion and reaction in this scenario. Nevertheless, it is obvious that the strand motion is closely related to the molecular structure. To further reduce the activation energy for strand motion and enhance the diffusivity, small cross-linkers in the form of stickers are introduced into the bond exchange reaction. In order to compare the adhesion ability,





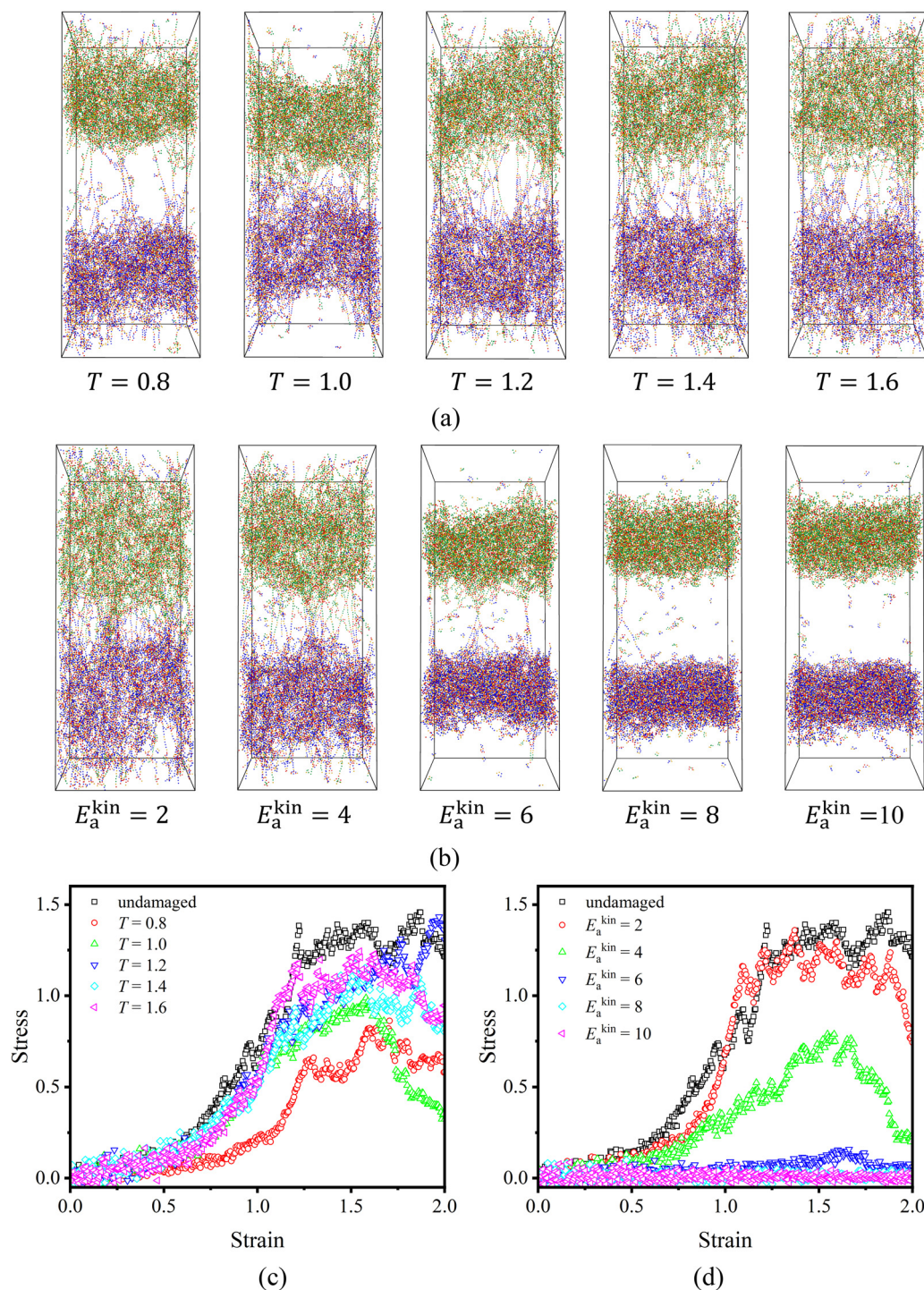


Fig. 6 Snapshots in the triaxial extension process and stress–strain curves at various temperatures ( $T$ ) (a) and (c) and activation energies ( $E_a^{\text{kin}}$ ) (b) and (d). Snapshots (a) and (b) depict the interfaces at  $t = 500\tau_{\text{LJ}}$ .

two sets of unentangled pendant crosslinked long linear chains ( $N = 50$ ) are designed, one with crosslinkers and the other without, but with the same crosslinking density. This comparison is shown in Fig. 7(a) and (b), respectively.

The snapshots shown in Fig. 8(a) and (b) reveal that much longer bridge chains can enhance the toughness through conformational transformation when extended. However, the

adhesion performance of the sample without crosslinkers deteriorates, requiring almost  $t = 50\,000\tau_{\text{LJ}}$  to achieve the same strength as the undamaged sample, as shown in Fig. 8(c). Despite having the same sticker content, the motion is restrained for longer chains, leading to higher activation energy for strand motion and hindering the adhesion behavior. In contrast, the addition of crosslinkers dramatically shortens





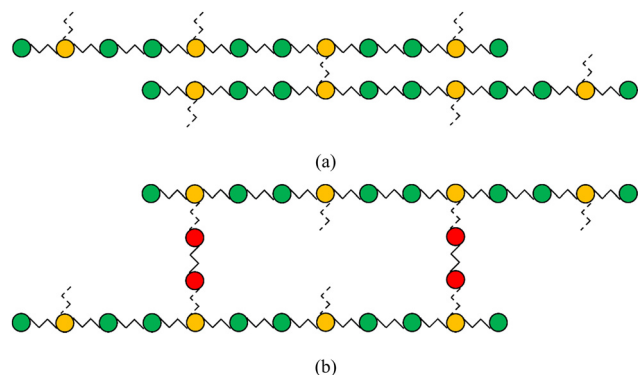


Fig. 7 Schematic description of the molecular design for long chains (a) without and (b) with crosslinkers. Green and yellow circles represent regular beads and stickers in the linear chain, respectively, and red circles represent the 2-mer crosslinker. Stickers can only additionally bond with one another sticker.

the adhesion time to  $t = 1000\tau_{LJ}$ , which is nearly 50 times quicker than the long-chain sample and only one time slower than the short-chain sample. This is evident that involvement of small molecules in chemical reactions accelerates the kinetics and shortens the relaxation time by bypassing the activation energy of strand motion. Note that the yield strain is  $\gamma_y \approx 3.5$ , representing a two-fold improvement compared to short-chain samples. However, the maximum stress is reduced to  $\sigma_{\max} \approx 1.0$ .

### 3.2. Diss-CANs for self-healing

Unlike self-adhesion, self-healing emphasizes the spontaneous healing behavior of the wound surface without any external intervention, but it requires even more universal conditions. An example from organisms is the healing of the skin. When the skin is damaged, it starts to heal as quickly as possible to stop bleeding. However, the newly healed skin usually has lower strength. In this case, fast local relaxation hence becomes crucial, and it is significantly different from self-adhesion.

The conservative crosslinking density of Asso-CANs provides enhanced creep resistance, while, reduction of crosslinks can actually prompt the healing performance. When subjected to external forces and deformation, Diss-CANs tend to dissociate into open stickers even before the strain rate reaches the inverse pre-factor of the terminal relaxation time.<sup>22</sup> These open stickers have a strong tendency to react with one another, facilitating easier healing even under challenging conditions like low temperatures. Local relaxation can be greatly accelerated through this mechanism.

The influence of the concentration of open stickers,  $C_{\text{open}}$ , on the bonding rate is investigated, as shown in Fig. 9. In the simulation, sticky bonds near the interface are removed partially or completely resulting in the presence of open stickers. It is found that under strong association energy ( $E_a^{\text{kin}} = 10\epsilon_{LJ}$ ) more than 90% of open stickers are bonded after  $t = 10^4\tau_{LJ}$ . This indicates that the presence of open stickers promotes bond formation, and the bonding rate increases with their content. As a result, the bonding rate at the interface is much faster than that in the bulk region due to the large number of exposed

bonding sites at the interface, as illustrated in Fig. S3 (ESI†). These findings support our claim that Diss-CANs are suitable for self-healing materials.

In our previous study, we found a strong correlation between the concentration of open stickers and the association energy.<sup>22</sup> In a weak-associated system, the interaction between stickers is not sufficiently strong to maintain them together, resulting in a significant presence of open stickers and hence poor healing behavior. To address this issue, it is crucial to establish a state of strong association that can promote effective self-healing. In Fig. 10, the equilibrium concentration of open stickers is plotted under various temperatures and activation energies. As the temperature decreases and the activation energy increases, the concentration of open stickers decreases accordingly. Here, to quantify the level of strong association, we define it as a state where the concentration of open stickers is below 10%.

The healing dynamics are investigated by comparing the changes in the concentration of open stickers at the interface with the corresponding mean-squared distance (MSD) under conditions of strong and weak association, as shown in Fig. 11. In the case of strong association, the concentration of open stickers decreases dramatically after some healing time, while for weak associations, it remains almost unchanged. Interestingly, the timescale at which the concentration of open stickers changes rapidly is similar to the timescale at which MSD reaches a plateau, indicating that the scale of the motion unit is predominantly strands. For Diss-CANs, this suggests that direct bonding between open stickers is the fastest mode of association. In contrast, no plateau is found for weak association, showing unhindered diffusion. This is actually why both  $N_{\text{bridge}}$  and  $d_{\text{bridge}}$  are used to quantify adhesion or the healing effect, as the depth of diffusion is insignificant for weak association. Evidently, stronger associations are necessary for the self-healing of Diss-CANs, which is opposed to the self-adhesion of Asso-CANs.

The stress-strain curves are plotted to examine the influence of various open sticker concentrations on the healing behavior of self-healing polymers at shorter healing time  $t = 100\tau_{LJ}$ , as shown in Fig. 12(a). It is observed that the level of open stickers has a great impact on the healing effect. For samples without open stickers that rely solely on dissociation and reassociation, the healing process did not commence within this time scale. Conversely, the samples with 80% open stickers exhibit almost half the strength compared to the undamaged sample, indicated by the maximum stress  $\sigma_{\max} \approx 0.7$ . Moreover, Fig. 12(b) shows the relationship between the concentration of open stickers and  $N_{\text{bridge}}$ , demonstrating a nearly proportional relationship.

Note that self-healing behavior is not limited to Diss-CANs. Asso-CANs also have open stickers on the damaged surface. However, it is generally believed that Diss-CANs exhibit superior healing performance to Asso-CANs. This is due to two key factors. Firstly, as discussed above, Diss-CANs tend to form more open stickers when damaged. Secondly, the bond exchange rate in Asso-CANs is not significantly affected by the presence of open stickers, whereas in Diss-CANs, open stickers



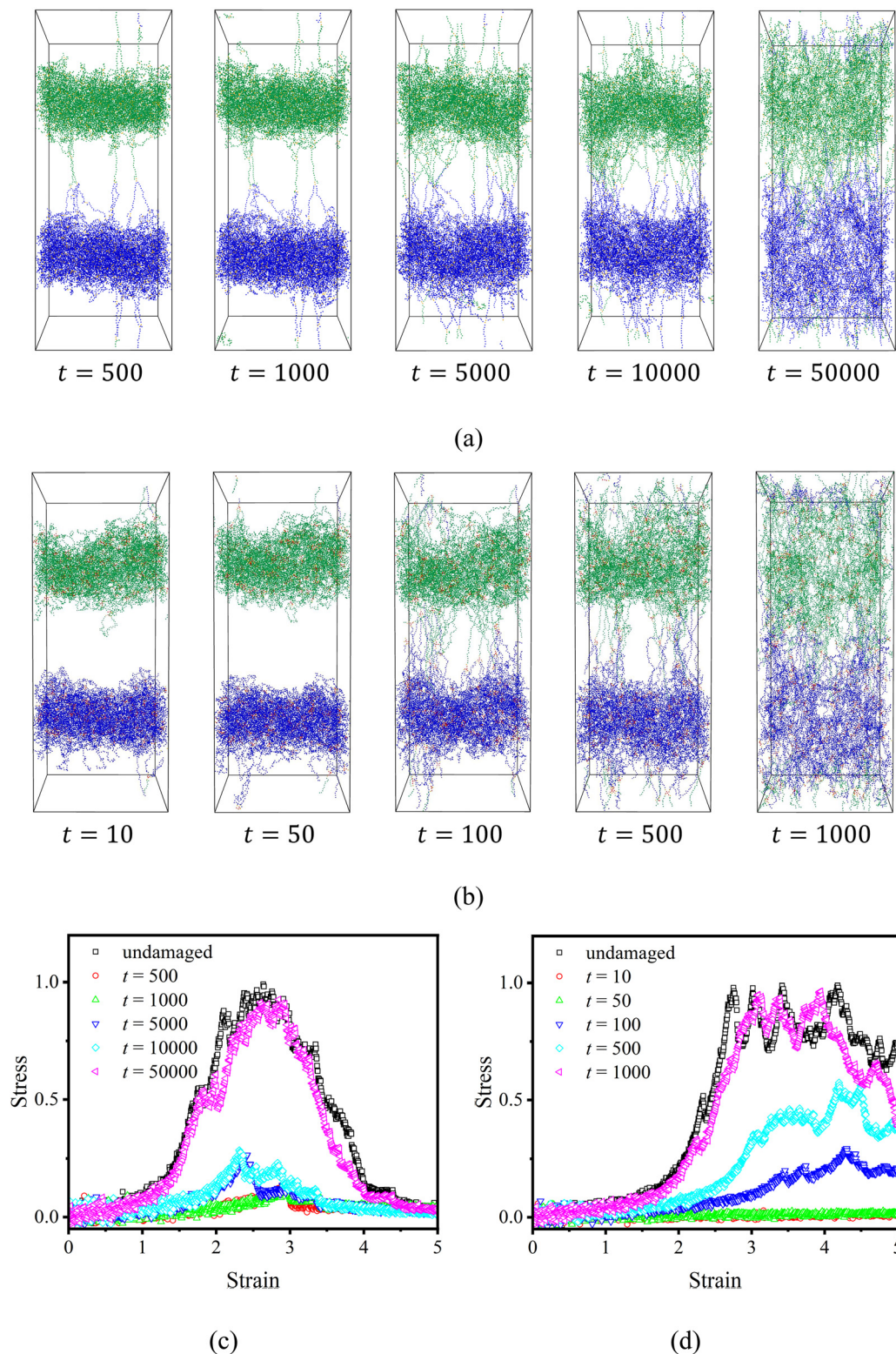


**Fig. 8** Extension process snapshots and stress–strain curves with long-chains without (a) and (c) and with crosslinkers (b) and (d). The types of beads are the same as in Fig. 7 and the blue beads represent the regular beads in the box below.

can easily bond together due to strong association energy. Wu *et al.*<sup>60</sup> conducted a study indicating that the influence of sticker concentration on healing performance is not as significant

as temperature or activation energy. Additionally, in some cases, Asso-CANs may have separate crosslinking and bond exchange reactions. In other words, it is uncertain whether the crosslinking



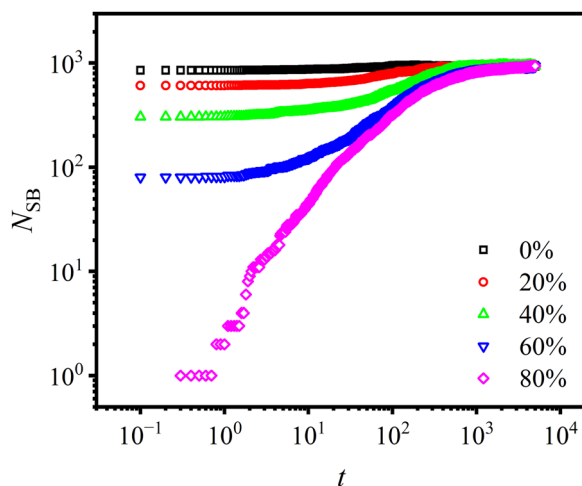


Fig. 9 Number of sticky bonds ( $N_{SB}$ ) formed near the interface as a function of time  $t$  under various concentrations of open stickers. Under strong association (activation energy  $E_a^{kin} = 10\varepsilon_{LJ}$ ), more than 90% of open stickers are bonded after bonding time  $t = 10^4\tau_{LJ}$ .

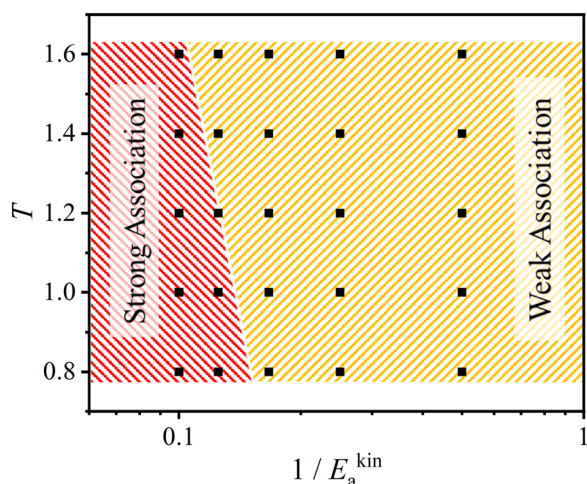


Fig. 10 Distinction of strong and weak association under various temperatures ( $T$ ) and activation energies ( $E_a^{kin}$ ). It is defined that under strong association, the concentration of open sticker is below 10%.

reaction can occur during the bond exchange reaction, resulting in the formation of open stickers that may not be able to participate in the rearrangement of the network.<sup>61</sup>

In addition, the healing efficiency can be influenced by the molecular structure. It is important to note that the dissociated small molecules remain unaffected by strand motion, resulting in a faster reaction rate. However, it is crucial to emphasize that the primary factor for self-healing is the kinetics of the chemical reaction. Therefore, we have provided less discussion on the molecular structure, focusing instead on the significance of reaction rates in the self-healing process.

### 3.3. Repair timescale of self-adhesion and self-healing processes

After conducting independent simulations, we have compared the timescale of self-adhesion for Asso-CANs and the

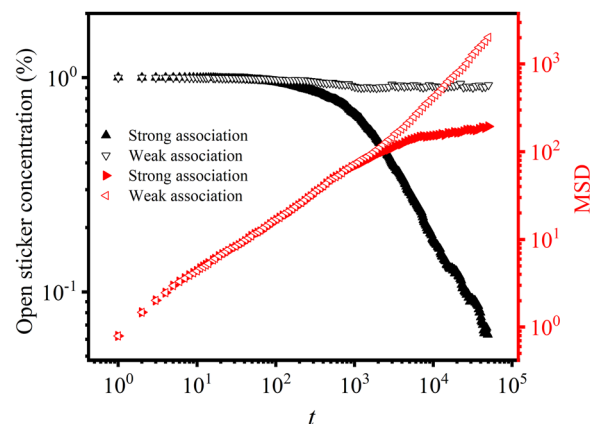


Fig. 11 Open sticker concentration as a function of time ( $t$ ) and its corresponding MSD for strong and weak associations.

self-healing for Diss-CANs theoretically. In the case of Asso-CANs, the repair (self-adhesion) timescale is solely determined by the bond exchange kinetics:

$$k_{BER} = A \exp\left(-\frac{E_{a,BER}}{k_B T}\right) \quad (5)$$

$$\tau_{s,BER} = \tau_{s,BER}^0 \exp\left(\frac{E_{a,BER}}{k_B T}\right) \quad (6)$$

where  $E_{a,BER}$  is the activation energy of the bond exchange reaction and  $\tau_{s,BER}$  is the terminal relaxation time of the network which can also be considered as the timescale for self-adhesion. The pre-factor in eqn (6) is related to the spatial distribution of stickers. Because of the four-body interaction, the exchange of a pair of bonded stickers can only occur when another pair of bonded stickers is encountered (Fig. 13(a)). As a result, the range of walking diffusion is limited, resulting in a smaller diffusion range compared to the length of strands. This limitation leads to a higher value for the pre-factor  $\tau_{s,BER}^0$ .

For the self-healing of Diss-CANs, as shown in Fig. 13(b), bond breakage becomes unnecessary, and we only need to consider the kinetics of bond creation. In this scenario, the repair timescale is solely dependent on the association between stickers. The reaction rate and corresponding relaxation time are as follows:

$$k_{create} = A \exp\left(-\frac{E_{a,create}}{k_B T}\right) \quad (7)$$

$$\tau_{s,BER} = \tau_{s,BER}^0 \exp\left(\frac{E_{a,BER}}{k_B T}\right) \quad (8)$$

where  $E_{a,create}$  is the activation energy of bond formation and  $\tau_{s,create} = 1/k_{create}$  is the healing timescale. It is known that the total activation energy is mainly controlled by bond breakage, and in the case of Diss-CANs, the value of  $E_{a,create}$  can be quite small. This implies that bond formation occurs swiftly. In addition, the range of walking diffusion in Diss-CANs exactly matches the length of strands, making it easier for an open





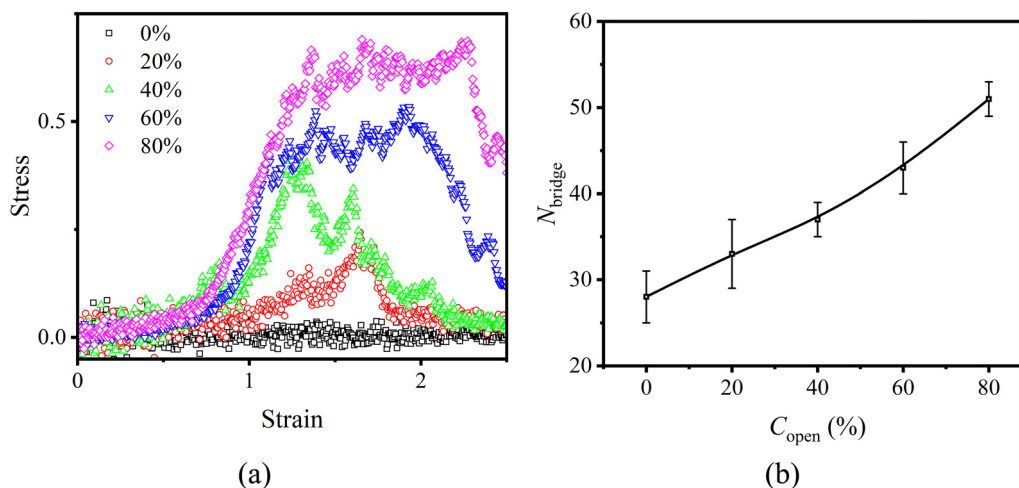


Fig. 12 (a) Stress–strain curves under various concentrations of open stickers. (b)  $N_{\text{bridge}}$  as a function of concentration of open stickers ( $C_{\text{open}}$ ).

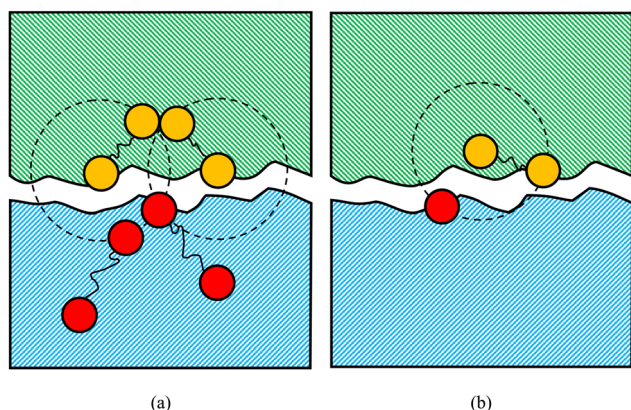


Fig. 13 Schematic diagram of (a) four-body bond exchange interactions in self-adhesion of Asso-CANs and (b) bond formation for self-healing in Diss-CANs. Stickers in different matrixes represented by yellow and red circles have the ability to associate with one another. The black dashed circles show the reaction radius of dangling chains.

sticker to encounter another, in contrast to Asso-CANs. As a result, the pre-factor value,  $\tau_{\text{s,create}}^0$  is comparatively smaller.

Therefore, considering both the activation energy and pre-factor in Arrhenius equation, it can be concluded that the repair timescale of Asso-CANs is generally slower than that of Diss-CANs when the molecular structure remains the same. However, this conclusion relies on the assumption that both damage and healing occur simultaneously at the interface of Diss-CANs. If the open stickers on one side of the interface cannot access the open stickers on the other side, they can deactivate by bonding to each other instead. Once the majority of the open stickers have transformed into bonded stickers after a characteristic time  $\tau_{\text{s,create}}$ , the self-healing behavior becomes indistinguishable from self-adhesion.

Polymer melt welding, similar to self-adhesion, involves the joining of entangled polymers. However, it requires higher temperatures and depends on long-distance diffusion for the

welding effect to occur. Consequently, the timescale for welding is generally closer to the terminal relaxation time of entangled polymers, which is typically slower than the repair timescale of CANs.

## 4. Conclusion

Building upon our previous work,<sup>22</sup> we utilize the linear and nonlinear viscoelastic properties of CANs to simulate the self-repair behavior by using a hybrid MC/MD algorithm. CANs exhibit diverse repair mechanisms, namely self-adhesion and self-healing, both of which are closely related to the kinetics of chemical reactions.

For self-adhesion, the emphasis is on bonding strength, as it determines the mechanical strength and creep resistance of Asso-CANs below  $T_v$ , making them suitable for self-adhesion materials. The kinetics play a crucial role in adhesion efficiency. Above  $T_v$ , the decrease of activation energy leads to an improved adhesion performance. By introducing small molecules, the adhesion time can be significantly reduced, as their diffusion is not affected by strand motion. At this point, the activation energy for viscous flow is almost equal to the activation energy for kinetics.

In self-healing materials, the local healing efficiency becomes the top priority. Dissociation is permitted, and the presence of open stickers on the damaged surface is inevitable, making Diss-CANs a suitable choice for self-healing materials perfectly. The healing process is primarily driven by the encounter of open stickers through walking diffusion across the surface. As a result, the healing efficiency is significantly influenced by the concentration of open stickers and the strength of association energy between them. Interestingly, in contrast to the self-adhesion behavior observed in Asso-CANs, an increase in the association energy actually improves the healing effect. Additionally, our work demonstrates that Diss-CANs exhibit a shorter self-healing timescale compared to the self-adhesion timescale observed in Asso-CANs. These findings



have significant implications for the development of self-repair materials, as they can serve as a valuable guide for understanding the molecular design of CANs to enhance their self-repairing capabilities.

## Conflicts of interest

There are no conflicts to declare.

## Acknowledgements

The authors acknowledge the financial support from the National Natural Science Foundation of China (grant no. 21973017 and 22373023).

## References

- 1 C. Jiang, L. Zhang, Q. Yang, S. Huang, H. Shi, Q. Long, B. Qian, Z. Liu, Q. Guan, M. Liu, R. Yang, Q. Zhao, Z. You and X. Ye, *Nat. Commun.*, 2021, **12**, 4395.
- 2 N. Tang, R. Zhang, Y. Zheng, J. Wang, M. Khatib, X. Jiang, C. Zhou, R. Omar, W. Saliba, W. Wu, M. Yuan, D. Cui and H. Haick, *Adv. Mater.*, 2022, **34**, 2106842.
- 3 Y. Liang, H. Xu, Z. Li, A. Zhangji and B. Guo, *Nanomicro Lett.*, 2022, **14**, 185.
- 4 H. Chen, Z. Z. Wu, Z. Su, S. Chen, C. Yan, M. Al-Mamun, Y. B. Tang and S. Q. Zhang, *Nano Energy*, 2021, **81**, 105654.
- 5 J. Xu, X. Wang, X. Zhang, Y. Zhang, Z. Yang, S. Li, L. Tao, Q. Wang and T. Wang, *Chem. Eng. J.*, 2023, **451**, 138673.
- 6 R. Guo, Q. Zhang, Y. Wu, H. Chen, Y. Liu, J. Wang, X. Duan, Q. Chen, Z. Ge and Y. Zhang, *Adv. Mater.*, 2023, **35**, 2212130.
- 7 W. J. Ma, Y. C. Ding, Y. S. Li, S. T. Gao, Z. C. Jiang, J. X. Cui, C. B. Huang and G. D. Fu, *J. Membr. Sci.*, 2021, **634**, 119402.
- 8 L. W. Ma, J. K. Wang, D. W. Zhang, Y. Huang, L. Y. Huang, P. J. Wang, H. C. Qian, X. G. Li, H. A. Terry and J. M. C. Mol, *Chem. Eng. J.*, 2021, **404**, 127118.
- 9 B. Li, S. Xue, P. Mu and J. Li, *ACS Appl. Mater. Interfaces*, 2022, **14**, 30192–30204.
- 10 P. Reutenauer, E. Buhler, P. J. Boul, S. J. Candau and J. M. Lehn, *Chemistry*, 2009, **15**, 1893–1900.
- 11 G. Du, A. Mao, J. Yu, J. Hou, N. Zhao, J. Han, Q. Zhao, W. Gao, T. Xie and H. Bai, *Nat. Commun.*, 2019, **10**, 800.
- 12 R. Xue, H. Zhao, Z. W. An, W. Wu, Y. Jiang, P. Li, C. X. Huang, D. Shi, R. K. Y. Li, G. H. Hu and S. F. Wang, *ACS Nano*, 2023, **17**, 5653–5662.
- 13 X. Y. Ding, G. Li, P. Zhang, E. Jin, C. S. Xiao and X. S. Chen, *Adv. Funct. Mater.*, 2021, **31**, 2011230.
- 14 X. Chen, M. A. Dam, K. Ono, A. Mal, H. Shen, S. R. Nutt, K. Sheran and F. Wudl, *Science*, 2002, **295**, 1698–1702.
- 15 C. Dry, *Compos. Struct.*, 1996, **35**, 263–269.
- 16 S. R. White, N. R. Sottos, P. H. Geubelle, J. S. Moore, M. R. Kessler, S. R. Sriram, E. N. Brown and S. Viswanathan, *Nature*, 2002, **415**, 817.
- 17 K. S. Toohey, N. R. Sottos, J. A. Lewis, J. S. Moore and S. R. White, *Nat. Mater.*, 2007, **6**, 581–585.
- 18 D. Montarnal, M. Capelot, F. Tournilhac and L. Leibler, *Science*, 2011, **334**, 965–968.
- 19 A. Jourdain, R. Asbai, A. Omaina, M. M. Chehimi, E. Drockenmuller and D. Montarnal, *Macromolecules*, 2020, **53**, 1884–1900.
- 20 L. E. Porath and C. M. Evans, *Macromolecules*, 2021, **54**, 4782–4791.
- 21 A. Rao, J. Ramirez and B. D. Olsen, *Macromolecules*, 2021, **54**, 11212–11227.
- 22 X. Cui, N. F. Jiang, J. Y. Shao, H. D. Zhang, Y. L. Yang and P. Tang, *Macromolecules*, 2023, **56**, 772–784.
- 23 M. Podgorski, B. D. Fairbanks, B. E. Kirkpatrick, M. McBride, A. Martinez, A. Dobson, N. J. Bongiardina and C. N. Bowman, *Adv. Mater.*, 2020, **32**, 1906876.
- 24 Y. H. Wu, S. Zhang, Y. Yang, Z. Li, Y. Wei and Y. Ji, *Sci. Adv.*, 2022, **8**, eabo6021.
- 25 S. S. Chen, M. Y. Zhang, Q. Y. Li, J. C. Li, S. P. Wu, J. Zhou, G. Q. Jin, Z. B. Zhang, X. Q. Pan and J. Zhu, *Macromolecules*, 2023, **56**, 5765–5773.
- 26 R. Dolog and R. A. Weiss, *Macromolecules*, 2013, **46**, 7845–7852.
- 27 W. Alabiso, T. M. Hron, D. Reisinger, D. Bautista-Anguis and S. Schlogl, *Polym. Chem.*, 2021, **12**, 5704–5714.
- 28 Y. C. Mao, Y. Kubota, R. Q. Feng, J. Gong, A. Ishigami, Y. Kobayashi, T. Watabe, D. Aoki, H. Otsuka and H. Ito, *Macromolecules*, 2022, **55**, 3948–3957.
- 29 J. R. Huang, N. Ramlawi, G. S. Sheridan, C. Chen, R. H. Ewoldt, P. V. Braun and C. M. Evans, *Macromolecules*, 2023, **56**, 1253–1262.
- 30 Y. J. Lin, Y. L. Chen, Z. A. Yu, Z. J. Huang, J. C. Lai, J. B. H. Tok, Y. Cui and Z. N. Bao, *Chem. Mater.*, 2022, **34**, 2393–2399.
- 31 H. L. Wang, Z. Shi, K. R. Guo, J. R. Wang, C. L. Gong, X. L. Xie and Z. G. Xue, *Macromolecules*, 2023, **56**, 2494–2504.
- 32 H. Guo, Y. Han, W. Zhao, J. Yang and L. Zhang, *Nat. Commun.*, 2020, **11**, 2037.
- 33 L. Imbernon, S. Norvez and L. Leibler, *Macromolecules*, 2016, **49**, 2172–2178.
- 34 S. Ciarella and W. G. Ellenbroek, *Coatings*, 2019, **9**, 114.
- 35 M. K. McBride, B. T. Worrell, T. Brown, L. M. Cox, N. Sowan, C. Wang, M. Podgorski, A. M. Martinez and C. N. Bowman, *Annu. Rev. Chem. Biomol.*, 2019, **10**, 175–198.
- 36 Y. Yang, H. M. Wang, S. Zhang, Y. Wei, X. M. He, J. L. Wang, Y. Y. Zhang and Y. Ji, *Matter*, 2021, **4**, 3354–3365.
- 37 N. Roy, B. Bruchmann and J. M. Lehn, *Chem. Soc. Rev.*, 2015, **44**, 3786–3807.
- 38 E. B. Stukalin, L. H. Cai, N. A. Kumar, L. Leibler and M. Rubinstein, *Macromolecules*, 2013, **46**, 7525–7541.
- 39 Z. R. Hinton, A. Shabbir and N. J. Alvarez, *Macromolecules*, 2019, **52**, 2231–2242.
- 40 Q. Chen, G. J. Tudryn and R. H. Colby, *J. Rheology*, 2013, **57**, 1441–1462.
- 41 N. F. Jiang, H. D. Zhang, P. Tang and Y. L. Yang, *Macromolecules*, 2020, **53**, 3438–3451.
- 42 N. F. Jiang, H. D. Zhang, Y. L. Yang and P. Tang, *J. Rheology*, 2021, **65**, 527–547.



- 43 J. Y. Shao, N. F. Jiang, H. D. Zhang, Y. L. Yang and P. Tang, *Macromolecules*, 2022, **55**, 535–549.
- 44 R. S. Hoy and G. H. Fredrickson, *J. Chem. Phys.*, 2009, **131**, 224902.
- 45 A. Perego and F. Khabaz, *Macromolecules*, 2020, **53**, 8406–8416.
- 46 A. Perego, D. Lazarenko, M. Cloitre and F. Khabaz, *Macromolecules*, 2022, **55**, 7605–7613.
- 47 K. Kremer and G. S. Grest, *J. Chem. Phys.*, 1990, **92**, 5057–5086.
- 48 R. Everaers, S. K. Sukumaran, G. S. Grest, C. Svaneborg, A. Sivasubramanian and K. Kremer, *Science*, 2004, **303**, 823–826.
- 49 A. P. Thompson, H. M. Aktulga, R. Berger, D. S. Bolintineanu, W. M. Brown, P. S. Crozier, P. J. I. Veld, A. Kohlmeyer, S. G. Moore, T. D. Nguyen, R. Shan, M. J. Stevens, J. Tranchida, C. Trott and S. J. Plimpton, *Comput. Phys. Commun.*, 2022, 271.
- 50 LAMMPS Home Page, (accessed 2023-08-02).
- 51 Z. Y. Zhang, J. Liu, S. Li, K. Gao, V. Ganesan and L. Q. Zhang, *Macromolecules*, 2019, **52**, 4154–4168.
- 52 Y. Fang, T. K. Yue, S. Li, Z. Y. Zhang, J. Liu and L. Q. Zhang, *Macromolecules*, 2021, **54**, 1095–1105.
- 53 J. He, Q. Chen, J. Qu, S. Li, Z. Fu, Y. Wei, S. Hu, A. Feng, L. Zhang and J. Liu, *ACS Appl. Poly. Mater.*, 2023, **5**, 3161–3172.
- 54 S. W. Sides, G. S. Grest and M. J. Stevens, *Phys. Rev. E: Stat., Nonlinear, Soft Matter Phys.*, 2001, **64**, 050802.
- 55 M. J. Stevens, *Macromolecules*, 2001, **34**, 2710–2718.
- 56 M. J. Stevens, *Macromolecules*, 2001, **34**, 1411–1415.
- 57 J. Rottler, S. Barsky and M. O. Robbins, *Phys. Rev. Lett.*, 2002, **89**, 148304.
- 58 C. Creton, E. J. Kramer, C. Y. Hui and H. R. Brown, *Macromolecules*, 1992, **25**, 3075–3088.
- 59 T. Yan, K. Schröter, F. Herbst, W. H. Binder and T. Thurn-Albrecht, *Macromolecules*, 2017, **50**, 2973–2985.
- 60 J. B. Wu, S. J. Li, H. Liu, H. J. Qian and Z. Y. Lu, *Phys. Chem. Chem. Phys.*, 2019, **21**, 13258–13267.
- 61 M. Rottger, T. Domenech, R. van der Weegen, A. Breuillac, R. Nicolay and L. Leibler, *Science*, 2017, **356**, 62–65.

